HHS Public Access

Author manuscript

Bone. Author manuscript; available in PMC 2024 December 01.

Published in final edited form as:

Bone. 2023 December ; 177: 116929. doi:10.1016/j.bone.2023.116929.

Optineurin Regulates Osteoblast Function in an Age-dependent Fashion in a Mouse Model of Paget's Disease of Bone

Xiangxiang Hu[*,1,2], **Brian L. Foster**[3], **Baohong Zhao**[4,5], **Henry C. Tseng**[6], **Yi-Chu Wu**[7], **Ching-Chang Ko**[*,2]

[1]Oral and Craniofacial Biomedicine Program, Adams School of Dentistry, University of North Carolina at Chapel Hill; Chapel Hill, NC, 27599, USA

[2]Division of Orthodontics, The Ohio State University College of Dentistry; Columbus, OH 43210, USA

[3]Division of Biosciences, The Ohio State University College of Dentistry; Columbus, OH, 43210, USA

[4]Arthritis and Tissue Degeneration Program and David Z. Rosensweig Genomics Research Center, Hospital for Special Surgery; New York, NY, 10021, USA

[5]Department of Medicine, Weill Cornell Medical College, Cornell University; New York, NY, 10065, USA

[6]Duke Eye Center and Department of Ophthalmology, Duke University Medical Center; Durham, NC, 27710, USA

[7]Division of Periodontology, The Ohio State University College of Dentistry; Columbus, OH 43210, USA

Abstract

Paget's disease of bone (PDB) is a degenerative disorder affecting the skull and bones. Hyperactive osteoclasts (OCs) initiate bone degradation in the early stage, followed by increased bone formation by osteoblasts (OBs) in trabecular bones during the advanced stage. This OB-OC uncoupling results in bone deformations and irregular trabecular bone patterns. Current mouse models poorly replicate the advanced-stage characteristics of PDB. Optineurin (Gene: *OPTN* in

[*]Correspondence: hu.2378@osu.edu (Xiangxiang Hu), ko.367@osu.edu (Ching-Chang Ko) Division of Orthodontics, The Ohio State University College of Dentistry, 305 w 12th Ave, Columbus, OH 43210, USA.

Declaration of competing interest

None.

Declaration of interests

The authors declare that they have no known competing financial interests or personal relationships that could have appeared to influence the work reported in this paper.

CRediT authorship contribution statement

Xiangxiang Hu: Formal analysis, Investigation, Writing – original draft. **Brian Foster:** Writing – review & editing. **Baohong Zhao:** Writing – review & editing. **Henry Tseng:** Writing – review & editing. **Yi-Chu Wu:** Writing – review & editing. **Ching-Chang Ko:** Writing – review & editing, Supervision, Funding acquisition.

humans, *Optn* in mice, protein: OPTN) has been implicated in PDB by genetic analyses. We identified PDB-like cortical lesions associated with OC hyperactivation in an *Optn* knockout ($Optn^{-/-}$) mouse model. However, the effects of OPTN dysfunction on OBs and trabecular bone in advanced PDB remain unclear. In this study, we used the $Optn^{-/-}$ mouse model to investigate trabecular bone abnormalities and OB activity in PDB. Micro-computed tomography analysis revealed severe pagetic alterations in craniofacial bones and femurs of aged $Optn^{-/-}$ mice, resembling clinical manifestations of PDB. Altered OB activity was observed in aged $Optn^{-/-}$ mice, implicating compensatory OB response in trabecular bone anomalies. To elucidate the role of OC-OB interactions in PDB, we conducted *in vitro* experiments using OC conditioned media (CM) to examine the effects on OB osteogenic potential. We found OC CM restored compromised osteogenic induction of $Optn^{-/-}$ bone marrow stromal cells (BMSCs) from young mice, suggesting OCs maintain OB activity through secreted factors. Strikingly, OC CM from aged $Optn^{-/-}$ mice significantly enhanced osteogenic capability of $Optn^{-/-}$ BMSCs, providing evidence for increased OB activity in advanced stages of PDB. We further identified TGF-β/BMP signaling pathway in mediating the effects of OC CM on OBs. Our findings provide insights into Optn's role in trabecular bone abnormalities and OB activity in PDB. This enhances understanding of PDB pathogenesis and may contribute to potential therapeutic strategies for PDB and related skeletal disorders.

Keywords

Osteitis Deformans; Models; Animal; Bone Remodeling; Osteogenesis; Osteoblasts; Aging

1. Introduction

Paget’s disease of bone (PDB) is a common degenerative bone disease affecting millions of elderly individuals [1, 2]. PDB is thought to be initiated by increased bone resorption by osteoclasts (OCs), resulting in focal resorptive lesions in cortical bone and disorganized trabecular bone [3]. Optineurin (Gene: OPTN in humans, *Optn* in mice, protein: OPTN) has been implicated by genetic analyses to be associated with PDB [4]. Gene-edited mouse models have had limited success in recapitulating key manifestations of PDB [1, 5]. To investigate the role of OPTN in PDB, we previously created an *Optn* global knock-out mouse ($Optn^{-/-}$) model [6]. Skeletal analyses revealed that aged (>16 month-old) $Optn^{-/-}$ mice exhibited hyperactivated OCs and PDB-like focal resorptive lesions in cortical bone [7, 8]. However, the trabecular bone aspect of the phenotype remained unclear.

PDB is initiated by hyperactivated osteoclasts and progressively worsens with age [3, 9]. The role of bone-forming osteoblasts (OBs) in the pathogenesis of PDB is unclear but potentially significant. In advanced stages of PDB, compensatory OB activity is thought to contribute to excess trabecular bone formation [10], resulting in abnormal and increased trabecular bone structures and cortical bone thickening [11]. The newly formed, disorganized bone tissue (woven bone) exhibits abnormal structure and poor bone quality, leading to manifestations that include increased head and jaw size, tooth malocclusion and mobility, curvature of the spine, and bowing of the limbs [12, 13]. This abnormal bone formation has not been well reproduced in current *Optn*-associated PDB mouse models

[14-16]. Some *in vitro* studies have suggested decreased OB activity in these mice [14, 17], adding further ambiguity to the role of OBs in Optn-associated PDB.

The mechanism(s) underlying loss-of-function of OPTN in the pathology of PDB remain undefined and several key questions remain unanswered. First, it is unclear how loss of *Optn* affects OB differentiation and function, and how this impacts trabecular bone. Second, the age-dependent alteration of OB activity and cause of trabecular bone disorganization remain unexplained. Lastly, the uncoupling of OCs and OBs during the onset of skeletal diseases like PDB are not fully understood. It is well established that OC and OB activities are coupled via secreted regulatory factors and juxtacrine pathways to coordinate bone remodeling [18]. OCs are strongly upregulated by OPTN loss-of-function both *in vitro* and *in vivo* [6-8, 19]. However, previous reports on OPTN function in mice do not provide a clear answer regarding the effect on OBs and OC-OB interactions in PDB model [6, 8, 14].

In this study, we identified pagetic, abnormal bone formation in the craniofacial bones and femurs of aged $Optn^{-/-}$ mice. We found that OB activity was altered in aged but not young $Optn^{-/-}$ mice. Our hypothesis was that OCs regulate the osteogenic potential of OBs in PDB development. To test this, we compared OBs from $Optn^{-/-}$ mice vs. their wildtype ($Optn^{+/+}$) littermates at a young age using an *in vitro* OC and OB co-culture approach. In young $Optn^{-/-}$ mice, OCs maintained OBs activity through secreted factors. Secretory factors from OCs of aged $Optn^{-/-}$ mice significantly increased OBs activity from the same mice, suggesting increased osteogenesis contributes to the skeletal phenotype of late-stage PDB. Furthermore, secretory factors from OCs activate transforming growth factor beta (TGF-β)/bone morphogenetic protein (BMP) signaling pathway in aged $Optn^{-/-}$ OB cells. Our findings improve understanding of abnormal bone remodeling in OPTN-associated PDB and provide insights into other skeletal disorders.

2. Materials and Methods

2.1. Mice

The generation of global *Optn* knockout ($Optn^{-/-}$) mice on a C57BL/6 background was described previously [6]. Heterozygous $Optn^{+/-}$ breeders generated $Optn^{+/+}$ (wild-type) mice and $Optn^{-/-}$ littermates. Males of both genotypes were randomly selected and analyzed at either 2 months (young) or 24 months (aged) for the *in vivo* and *in vitro* analyses described below. For phenotype analyses, ten male $Optn^{+/+}$ and $Optn^{-/-}$ mice were compared. For bone histology and serum ELISA assays, four male $Optn^{+/+}$ and $Optn^{-/-}$ mice were compared. All of the *in vitro* results were based on cells cultured from at least three mice of each genotype. All animal procedures were approved by the Institutional Animal Care and Use Committees at the University of North Carolina at Chapel Hill, Duke University, and the Ohio State University (2020A00000064-R1). All animal experiments comply with the ARRIVE guidelines.

2.2. Primary cell isolation

Eight-week-old and 24-month-old $Optn^{+/+}$ and $Optn^{-/-}$ mice were euthanized by CO_2. Femurs, tibias, and humeruses were collected and bone marrow cells were flushed out

into α–minimum essential medium (α–MEM) containing 20% fetal bovine serum (FBS) and penicillin/streptomycin. The mixed cells were maintained at 37°C in a humidified 5% CO_2 atmosphere. After 2 days, non-adherent cells were removed (and collected for further use). The adherent cells were cultured by changing the culture medium every 3 days until passaging when cells reached 80% confluence. The passaged cells were maintained by changing culture medium every 2 days. Passage 2 cells were used for in vitro experiments described below.

2.3. Identification of bone marrow stromal cells

Bone marrow stromal cells (BMSCs) were identified by flow cytometry for isolation [20]. Passage 2 cells were trypsinized, counted, suspended in phosphate buffered saline (PBS) containing 5% bovine serum albumin (BSA) (5×10^5 cells/30 μL), and then incubated with PE-conjugated antibodies against CD90, CD105, Sca-1, CD31, and CD45 at 4°C for 30 min. Negative control cells were stained with PE-conjugated mouse IgG1 isotype (BD Biosciences). Expression of BMSC surface markers ($CD90^+$, $CD105^+$, $Sca\text{-}1^+$, $CD31^-$, $CD45^-$) was evaluated with a FACS Calibur flow cytometer using CellQuest Pro (BD Biosciences) software. For more information, please see the Supplemental Table 1.

2.4. Cell viability assay

BMSCs were measured by the MT Cell Viability Assay (Promega) according to the manufacturer's directions. Briefly, a suspension of passage 2 BMSCs was prepared by adding MT Cell Viability reagents to the culture media. Cells were seeded in this medium and cultured for 3 days. Luminescence of treated cells was measured via a Cytation 5 plate reader (BioTek). Supplemental Table 1.

2.5. Cell death/apoptosis assay

BMSCs were measured by Dead Cell Apoptosis Kits with Annexin V for Flow Cytometry according to the manufacturer's directions (Invitrogen™). Briefly, a suspension of passage 2 BMSCs was stained with Annexin V and propidium iodide provided in the kit and evaluated with a FACS Calibur flow cytometer using CellQuest Pro (BD Biosciences) software. For more information, see the Supplemental Table 1.

2.6. Preparation of (pre)osteoclasts conditioned media

Non-adherent cells described in the primary culture of BMSCs were collected and reseeded in a 6-well culture plate at the concentration of 2 x 10^5 cells/mL and 1.5 mL/well. Cells were cultured with α–MEM as previously described (containing 20% FBS and penicillin/streptomycin), with the addition of 60 ng/mL macrophage colony-stimulating factor (M-CSF) at for 3 days to promote the growth of OC precursors. On day 3, the α–MEM culture media were replenished with media containing 60 ng/mL M-CSF and 20 ng/mL RANKL for another 5 days to promote OC differentiation. Each well was filled with 2.5 mL of media to prevent drying out. The media were then collected and concentrated using centrifugal filter units (Millipore Sigma) to a concentration factor of 25x (2.5 mL to 100 μL per well) and stored at −80 °C for further use.

2.7. Osteogenic differentiation

To promote osteogenic differentiation, BMSCs were cultured in 6-well plates (for RT qPCR assays) or 12-well plates (for staining Alizarin Red S) with osteogenic media. Osteogenic media was composed of BMSC culture media (α–MEM with 20% FBS and penicillin/streptomycin) containing 50 μg/ml ascorbic acid (MilliporeSigma), 10 mM β-glycerophosphate (MilliporeSigma), and 10 nM dexamethasone (MilliporeSigma). Osteogenic media were replenished every 3 days for a total of 7, 14, or 21 days. PreOC conditioned media were added at 100 μL per well for 6-well plates and at 50 μL per well for 12-well plates, when indicated.

2.8. Micro–computed tomography

Micro-computed tomography (μCT) scanning was performed following established protocols described previously [6, 8]. Femurs were dissected from mice free of soft tissue, fixed overnight in 4% paraformaldehyde, and analyzed by μCT (1172-D Skyscan) with the following scanning parameters: 10-μm^3 voxel size, 50 kVp, 200 μA, 0.4° rotation per projection, eight frames averaged per projection, and 260-ms exposure time. Reconstruction was performed using NRecon software. The trabecular bone region of interest (ROI) was drawn starting from 5% of femoral length proximal to distal epiphyseal growth plate and extended proximally for a total of 5% of femoral length. The trabecular bone was segmented from the bone marrow and analyzed to determine the trabecular bone volume fraction (Tb. BV/TV), trabecular bone mineral density (Tb. BMD), trabecular thickness (Tb. Th), trabecular number (Tb. N), and trabecular spacing (Tb. Sp). The cortical bone ROI was drawn in the middle shaft approximately 1/3 of the full femur length. The cortical bone was segmented from the trabecular bone and analyzed to determine the cortical bone mineral density (Ct. BMD), cortical thickness (Ct. Th), and cortical bone area (Ct. Ar).

2.9. ELISA assays

A serum-based ELISA assay was performed to test levels of circulating bone alkaline phosphatase (BALP). As described previously [8], whole blood was collected by cardiac puncture at the time of euthanasia. Blood was allowed to clot at 4°C overnight, followed by centrifuging at 3,000 rpm for 15 min. The serum supernatant was carefully collected for ELISA assays. The mouse BALP ELISA Kit (MyBioSource) was used following the manufacturer's protocol. Supernatant-based ELISA assays were performed to test levels of transforming growth factor-beta (TGF-β) and Interleukin 6 (IL-6), in osteoclast conditioned media (OC CM). Conditioned media were concentrated using centrifugal filter units (MilliporeSigma) to a concentration factor of 5x for ELISA assays. The mouse TGF-β and IL-6 kits were used following the manufacturer's protocol (Invitrogen). For more information, see Supplemental Table 1.

2.10. Cell and tissue staining

For tartrate-resistant acid phosphatase (TRAP) staining, solutions were prepared following a previously published standard protocol. Cells were fixed with 10% paraformaldehyde for 10 min before incubating in TRAP staining solution for 10 min at 37°C. For Alizarin Red staining, cells were fixed with 10% paraformaldehyde for 10 min and

incubated in 1% Alizarin Red stain for 10 min, followed by three washes. Bound alizarin red was eluted using a solution of 20% methanol and 10% acetic acid in water and absorbance was analyzed on a spectrophotometer at a wavelength of 405 nm. For H&E staining of femur sections, paraffin-embedded slices were deparaffinized and stained with Hematoxylin (Gill no. 2; GHS216-500ML, MilliporeSigma) and Eosin Y solution (HT110116-500ML, Millipore Sigma) following the manufacturer's instructions. Stained sections were imaged using an Eclipse Ti microscope (Nikon). The thickness of metaphysis (Thickness. metaphysis) was also measured using H&E stained images of coronal sections cutting through the mid-line of the femurs.

2.11. Alkaline phosphatase staining

As previously described [8, 21], 20 μm cryo-sectioned femur slices were prepared. For immunostaining, slices were permeabilized with 0.3% Triton X-100 for 10 min and washed three times with PBS. After blocking with PBS solution with normal donkey serum (566460, MilliporeSigma) for 1 hour, slices were incubated with tissue-nonspecific alkaline phosphatase (ALP) primary antibodies (Biotechne) at a concentration of 1:50 in PBS overnight at 4°C. The slices were then washed three times and incubated with donkey anti-goat IgG secondary antibody (A-11055) at a concentration of 1:200 in PBS containing 20% donkey serum for 2 hours at room temperature. The slices were mounted with 70% glycerin and imaged by an A1R confocal microscope system (Nikon). Each image was quantified using ImageJ by assigning the "brightness" window in color threshold setting. The length of ALP positive signal that passed the brightness threshold in each image was picked up and recorded. Each analysis was done three times to determine statistical significance.

2.12. mRNA sequencing and bioinformatic analysis

As described previously [8, 22], total RNA of was extracted using an RNeasy mini kit (Qiagen). For comparison between the BMSCs treated with different (pre)OC conditioned media, RNA sequencing (RNA-seq) analyses were performed on *Optn*$^{+/+}$ and *Optn*$^{-/-}$ cells treated with OC CM (3 samples/group). A cDNA library was prepared using NEBNext Ultra DNA library prep kit (New England Biolabs) and mRNA sequencing was performed on the NovaSeq 6000 System (Illumina). Reads were mapped to the *Mus musculus* mm10 genome by STAR software. Fragments per kilobase of transcript per million mapped reads were calculated to estimate gene expression levels. Differential expression (DE) analysis was performed using the DESeq2 package in R software to identify the significant DE genes in the comparisons. *P*-values were adjusted using the Benjamini and Hochberg procedure for controlling the false discovery rate. Gene set enrichment tests were performed using the clusterProfiler package and the "camera" function in limma package in R software to test gene sets in KEGG collection.

2.13. Reverse transcription quantitative polymerase chain reaction

Total RNA of BMSCs was isolated using RNAzol and reverse-transcribed using the iScript Kit. PCR reactions were prepared using the iTaq Universal SYBR Green Supermix and performed on the StepOnePlus Real-Time PCR System (Applied Biosystems). Primers for target genes are listed in Supplemental Table 2. Threshold cycles of primers were

normalized to a housekeeping gene (β-actin), and the relative values were calculated on the basis of comparative Ct method (2 - $\Delta\Delta C_t$ method).

2.14. Statistical analyses

Statistical analyses were performed using Prism 9 (GraphPad Software, San Diego, CA). Significance was determined as $P<0.05$. Comparisons with a specific control were assessed using Student's t-test or one-way analysis of variance (ANOVA), followed by post hoc Bonferroni's correction. Data are expressed as means ± SD. P-values in figures are signified by $*P < 0.05$, $**P < 0.01$, or ***P < 0.001.

3. Results

3.1. Deletion of *Optn* contributes to pagetic alterations in skulls and femurs of aged mice

Previous studies have revealed PDB-like cortical focal lesions on the skulls and long bones of aged *Optn*$^{-/-}$ mice [6]. To investigate age-related effects on the craniofacial and femoral trabecular bone phenotype, we performed micro-computed tomography (micro-CT) analysis on skulls and femurs of ten 24-month-old *Optn*$^{-/-}$ male mice. There were no significant differences in body length or weight between genotypes (Supplemental Fig. 1).

All ten skulls from aged male *Optn*$^{-/-}$ mice exhibited thickened calvaria, a common craniofacial manifestation in PDB (Fig. 1A, E). Additionally, four skulls had thickened but translucent alveolar and mandibular bone (Fig. 1B, E), and two skulls showed deformed and enlarged structures (Fig. 1C, E), representing severe craniofacial manifestations in late-stage PDB. Among the ten femurs, eight exhibited disorganized epiphyseal trabeculae (marked as 1 in Figure 1D, E). All femurs showed trabecularization of the metaphyseal line (marked as 2 in Figure 1D, E) and trabecularization of the cortical bone structure (marked as 3 in Figure 1D, E), particularly close to the metaphyseal line. Two femurs displayed significantly increased but irregular trabecular bone, resembling the mosaic pattern observed in some late-stage PDB patients (marked as 4 in Figure 1D, E).

Quantitative analysis of femurs revealed significant alterations in cortical bone parameters. The bone mineral density (Ct. BMD) decreased, and cortical thickness (Ct. Th) increased in *Optn*$^{-/-}$ mice (Fig. 1F). Trabecular bone density parameters were variable in 24-month-old *Optn*$^{-/-}$ mice (Fig. 1G). Tb. Sp was decreased, and trabecular number (Tb. N) was increased compared to *Optn*$^{+/+}$ mice, while other parameters remained unchanged (Fig. 1G). These trabecular parameters confirmed the irregular formation of trabecular bones in aged *Optn*$^{-/-}$ mice, resembling clinical features of PDB. Our data indicate the *Optn*$^{-/-}$ mouse model phenocopies irregular trabecular bone features of advanced PDB and may serve as a model to study the underlying pathological mechanisms.

3.2. Deletion of *Optn* leads to altered osteoblast activity in aged mice

Compensatory OB activity is believed to contribute to the disorganized trabecular bone in PDB [12]. To contextualize the micro-CT findings in relation to trabecular bone and OBs in aged mice, we analyzed femurs from *Optn*$^{-/-}$ and *Optn*$^{+/+}$ mice at 24 months. H&E staining revealed disorganized epiphysis (Fig. 2A, row 1) and smaller, irregularly distributed

trabeculae (Fig. 2A, row 2) in aged *Optn*$^{-/-}$ mouse femurs compared to *Optn*$^{+/+}$ femurs. Woven bone, a characteristic feature of PDB, could also be observed in aged *Optn*$^{-/-}$ mouse femurs (Supplemental Fig. 2). Immunostaining for the OB marker TNAP showed discontinuous labeling along the epiphyseal line in aged *Optn*$^{-/-}$ mice (Fig. 2B, row 1). Increased TNAP localization was observed in the spaces between trabeculae in aged *Optn*$^{-/-}$ mice (Fig. 2B, row 2), and TNAP signal length was trending high in aged *Optn*$^{-/-}$ mice (Fig. 2C). Circulating BALP, a marker of OB activity and bone turnover, was significantly elevated by approximately 25% in aged *Optn*$^{-/-}$ mice (Fig. 2D).

In our previous study, *Optn*$^{-/-}$ mice under 16 months-of-age did not exhibit any PDB-like phenotypes. Continuing our studies, we compared trabecular structure and OBs in the femurs of 2-month-old *Optn*$^{-/-}$ and *Optn*$^{+/+}$ mice. Similar to the aged mice, there were no significant differences in body length or weight between genotypes (Supplemental Fig. 1). H&E staining revealed no substantial differences in bone structure between young *Optn*$^{-/-}$ and *Optn*$^{+/+}$ mice (Fig. 2E). Immunostaining for TNAP and confocal imaging confirmed similar OB activity between genotypes (Fig. 2F, G) and circulating BALP did not differ between 2-month-old *Optn*$^{-/-}$ and *Optn*$^{+/+}$ mice (Fig. 2H). These findings supported that advanced age is required to manifest OB alterations associated with trabecular bone changes in Optn$^{-/-}$ mice, consistent with the trabecular abnormalities observed in PDB patients.

3.3. Osteoclast secreted factors restore compromised *in vitro* osteogenic induction of BMSCs from young *Optn*$^{-/-}$ mice

A previous *in vitro* study reported that deletion of *Optn* leads to decreased osteogenic potential in neonatal OBs [17]. In contrast, our collective local and systemic data suggest that bone mass is not significantly affected in young bones [6, 8]. To investigate this further, we determined whether deletion of *Optn* decreases osteogenic potential of bone marrow stromal cells (BMSCs), the progenitors of osteoblasts, obtained from young mice.

We established primary cultures of BMSCs from 2-month-old mice of *Optn*$^{-/-}$ and *Optn*$^{+/+}$ and identified them at passage two (P2) (Supplemental Fig. 3A). The BMSCs exhibited similar morphology (Supplemental Fig. 3B), cell viability (Supplemental Fig. 3C), and apoptotic or necrotic cell numbers (Supplemental Fig. 3D), regardless of the genotype. BMSCs were provided with osteogenic media and analyzed at 7, 14, and 21 days by PCR analysis (Fig. 3A). Expression of key osteogenic markers, including RUNX family transcription factor 2 (*Runx2*), *Alpl*, and osteocalcin (*Bglap/Ocn*), were significantly decreased in *Optn*$^{-/-}$ versus in *Optn*$^{+/+}$ (Fig. 3B). Additionally, *Optn*$^{-/-}$ BMSCs deposited significantly reduced quantities of mineral compared to *Optn*$^{+/+}$ BMSCs at day 21 following osteogenic induction, as shown by Alizarin Red S staining (Fig. 3C).

Considering that pre-osteoclasts (preOCs; in the monocyte-macrophage hematopoietic lineage) and OCs regulate osteoblastogenesis and OB function via secreted factors *in vivo* [23], we examined the effect of OC conditioned media (CM) on OB phenotype in the absence of *Optn*. Primary monocytes and BMSCs were isolated from 2-month-old *Optn*$^{-/-}$ or *Optn*$^{+/+}$ mice. Monocytes were grown for 5 days, stimulated with receptor activator of NF-κB ligand (RANKL) to induce osteoclastogenesis, and CM were collected (Figure 3D). After induction, we observed that *Optn*$^{-/-}$ preOCs produced more mature OCs

(Supplemental Fig. 4A), and gene expression of several key OC markers, including nuclear factor of activated T cells 1 (*Nfatc1*), cathepsin K (*Ctsk*), and transcription factor, *cFos*, were significantly increased compared to *Optn*$^{+/+}$ OC cells (Supplemental Fig. 4B).

CM from either *Optn*$^{-/-}$ or *Optn*$^{+/+}$ OCs were administered to BMSCs of the same genotype undergoing osteogenic induction and osteogenesis was evaluated at 7, 14, and 21 days, as previously outlined (Fig. 3D). With addition of CM, no significant differences in OB markers (*Runx2*, *Alpl*, and *Bglap/Ocn*) were noted in BMSCs treated with OC CM from the same genotype (Fig. 3E). Alizarin Red S staining also revealed no differences in calcium deposits between the two culturing systems (Fig. 3F).

Next, OC CM were added to BMSCs of the opposite genotype during osteogenic induction (i.e. *Optn*$^{-/-}$ OC CM to *Optn*$^{+/+}$ BMSC and *Optn*$^{+/+}$ OC CM to *Optn*$^{-/-}$ BMSC as illustrated in Fig. 3G). Again, no differences were found in OB marker expression (Fig. 3H) or mineral deposition (Fig. 3I) based on cross treatment with OC CM from 2-month-old mice.

Collectively, these experiments showed that there are no differences in secreted factors released by either *Optn*$^{-/-}$ or *Optn*$^{+/+}$ OCs into the culture media. The finding that *Optn*$^{-/-}$ BMSCs had lower differential potential into mature OBs but could be restored by CM suggested that OCs maintains OBs activity through secreted factors in young *Optn*$^{-/-}$ mice.

3.4. Osteoclasts secrete factors increase *in vitro* osteogenic induction of BMSCs from aged *Optn*$^{-/-}$ mice

Clinical reports suggest increased OB activity contributes to disorganized trabecular bone structures in advanced stages of PDB [12]. However, increased OB activity has not been confirmed by *in vitro* assays in PDB models and no mechanism has been proposed. We tested whether advanced age influences osteogenic differentiation in *Optn*$^{-/-}$ vs. *Optn*$^{-/-}$ BMSCs isolated from 24-month-old mice (Fig. 4A). Regardless of genotype, aged BMSCs exhibited similar morphology, viability, and similar numbers of apoptotic or necrotic cells (Supplemental Fig. 3 B-D). Osteogenic induction led to no significant differences in OB marker gene expressions for *Runx2*, *Alpl*, or *Bglap/Ocn* at 7, 14, or 21d (Fig. 4B). Alizarin Red S staining revealed no difference in calcium deposition from *Optn*$^{-/-}$ and *Optn*$^{+/+}$ OBs (Fig. 4C).

To explore the effects of OCs on the OB phenotype in the absence of *Optn*, BMSCs and OCs were derived from 24-month-old mice. Induction of monocytes from *Optn*$^{-/-}$ mice yielded a higher number of OCs (Supplemental Fig. 4A) and increased expression of OC markers (Supplemental Fig. 4B) compared to *Optn*$^{+/+}$ monocytes. CM was collected for use in treating OBs.

BMSCs from 24-month-old *Optn*$^{-/-}$ or *Optn*$^{+/+}$ mice were treated with CM from their respective same-aged OCs and were evaluated at 7, 14, and 21 days (Fig. 4D). Surprisingly, expression of key OB markers, *Runx2*, *Alpl*, and *Bglap/Ocn*, was significantly higher in *Optn*$^{-/-}$ vs. *Optn*$^{+/+}$ cells. Alizarin Red S staining indicated more than 2-fold increased mineral deposition by *Optn*$^{-/-}$ OBs following exposure to CM from OCs (Fig. 4F).

Next, CM from OCs derived from 24-month-old mice were added to BMSCs of the opposite genotype during osteogenic induction (i.e. *Optn*$^{-/-}$ OC CM to *Optn*$^{+/+}$ BMSC and *Optn*$^{+/+}$ OC CM to *Optn*$^{-/-}$ BMSC as illustrated in Fig. 4G). This approach reversed the trend and *Optn*$^{+/+}$ cells induced by *Optn*$^{-/-}$ OC CM exhibited increased expression of OB markers at some time points (Fig. 4H). Alizarin Red S staining revealed increased calcium deposition by *Optn*$^{+/+}$ cells induced by *Optn*$^{-/-}$ OC CM (Fig. 4I).

Collectively, data from these experiments demonstrated that OCs purified from 24-month-old *Optn*$^{-/-}$ mice induce a higher level of OB activity. Furthermore, these CM experiments suggested that this effect is mediated by one or more factors secreted by OCs into the surrounding culture media (such as cytokines and miRNA). Interestingly, this effect was not observed in OCs purified from 2-month-old mice (above section). However, it is unclear whether the effect is due to bulk increase in release of cytokines in presence of higher number of OCs in *Optn*$^{-/-}$ cultures versus age-dependent changes in OC/OBs that alters cytokine production or response.

3.5. Osteoclast secreted factors trigger TGF-β/BMP pathway signaling in aged *Optn*$^{-/-}$ mice

To begin to identify mechanisms by which OCs may influence OB activity and osteogenesis in *Optn*$^{-/-}$ mice, we investigated transcriptional changes in OCs and OBs that might indicate altered cytokine production or response. We accomplished this by performing RNA-seq to analyze transcriptomes of *Optn*$^{-/-}$ BMSCs treated with *Optn*$^{-/-}$ OC CM to the same cells treated *Optn*$^{+/+}$ OC CM. RNA was collected from BMSCs undergoing osteogenic induction in the presence of OC CM for 7 days (Fig. 5A). We identified 240 up-regulated genes and 255 down-regulated genes in BMSCs treated with *Optn*$^{-/-}$ OC CM vs. *Optn*$^{+/+}$ OC CM (Fig. 5B). KEGG pathway analysis revealed altered expression of multiple genes in pathways related to T-cells and osteoclasts (Fig. 5C). Notably, genes of the TGF-β/ BMP signaling pathway, which regulates osteoblast differentiation [24, 25], were up-regulated, including *Bmp*, *Bmp2/4*, *Smad1/5/8*, and *Smad4* (Supplemental Fig. 5). Gene set enrichment analysis (GSEA) of the differentially expressed genes further confirmed involvement of the TGF-β signaling pathway ($P < 0.005$ and FDR = 0.110) in BMSCs treated by the *Optn*$^{-/-}$ OC CM (Fig. 5D). qPCR assays indicated that OC CM from either genotype upregulated TGF-β signaling-associated markers, *Bmp2*, *Bmp6*, *Smad1* and *Smad5*. Up-regulation of these genes was greatest with *Optn*$^{-/-}$ OC CM in treated BMSCs (Fig. 5E). Finally, we tested the concentrations of TGF- β and interleukin 6 (IL-6), another secretory factor that has been corelated with PDB, in the OC CM collected from aged osteoclasts. We found that TGF-β expression was significantly higher in *Optn*$^{-/-}$ OC CM vs. *Optn*$^{+/+}$ OC CM. We did not observe any difference in IL-6 expressions (Fig. 5F). Collectively, our data suggested the TGF-β/BMP signaling pathway is involved in mediating the regulatory effects of *Optn*$^{-/-}$ OCs on the osteogenesis of OBs and could contribute to abnormal bone formation in advanced stages of PDB (Fig. 5G).

4. Discussion

Paget's disease of bone (PDB) is one of the most common degenerative bone diseases, yet remains poorly understood due to lack of well-established animal models [2, 12]. Current understanding of PDB pathogenesis hinges on hyperactivation of osteoclasts (OCs) resulting from mutations in OC regulatory genes and compensatory upregulation of osteoblasts (OBs) through direct or indirect mechanisms that have not yet been elucidated [11, 26, 27]. Optineurin (*Optn*) was identified as a candidate contributory gene for PDB [4], with genetic variants in humans and genetic deletion in mice associated with PDB bone lesions and OC hyperactivity [6, 19, 28, 29]. While several mouse models have been developed to study the impact of OPTN on OC [6, 7, 19] and OB [14, 17] activities and age-dependent pagetic abnormalities, some of these models show significant trabecular bone loss in young age [14, 17]. The current study addresses key knowledge gaps on how loss of OPTN affects trabecular bone, OB, and OC-OB interaction in PDB. Using the *Optn* global knockout mouse model [6, 8], we discovered severe trabecular bone abnormalities in the skulls and femurs of aged $Optn^{-/-}$ mice, and we associated these changes with increased OB activity *in vivo*. However, *in vitro* experiments revealed that OB activity decreased in young $Optn^{-/-}$ mice and remained unchanged in aged $Optn^{-/-}$ mice. To explain the discrepancy, we investigated the role of OC-OB interactions in regulating osteogenesis. We found OC CM restored compromised osteogenic induction of $Optn^{-/-}$ BMSCs from young mice, suggesting OCs maintain OB activity through secreted factors. Strikingly, OC CM from aged $Optn^{-/-}$ mice significantly enhanced osteogenic capability of $Optn^{-/-}$ BMSCs, which matched the skeletal phenotypes observed in aged $Optn^{-/-}$ mice, providing evidence for increased OB activity in advanced stages of PDB. Finally, we implicated increasing TGF-β/BMP signaling pathway in aged $Optn^{-/-}$ OBs, which is linked to the trabecular abnormalities in aged $Optn^{-/-}$ mice (Fig. 5G).

PDB is initiated by hyperactivated osteoclastogenesis and the formation of focal resorptive lesions [3, 9, 30]. Unlike osteoporosis, which is characterized by inhibited osteogenesis with age, PDB is characterized by increased bone turnover and disordered bone structure [1, 31]. In this study, we observed robust pagetic structural changes in craniofacial bones and femurs of aged $Optn^{-/-}$ mouse, confirming global *Optn*-exon 1 deletion as a reliable mouse model of PDB. Two recently reported *Optn* (exon 3 and 8) deletion mouse models exhibited bone loss at a young age but lacked pathological PDB lesions associated with resorption activities [14, 17]. Previous mouse models harboring specific point mutations in *Optn*, including the $Optn^{D477N/D477N}$ and $Optn^{\Delta ex12/\Delta ex12}$ mice, showed very limited or no PDB bone lesions [32]. Additionally, mice with *Optn* conditional knockout (Sox2-CRE) and $Optn^{D477N/D477N}$ mutation did not show bone degeneration [15, 16]. As shown in Supplemental Table 3 the $Optn^{-/-}$ mouse model described here provides a good translational model for *Optn*-associated PDB.

OC secretions, an important mechanism of OC-OB interactions, have been suggested to contribute to PDB pathogenesis in a measles virus model of PDB, where OCs release high levels of interleukin-6 (IL-6) to enhance osteogenesis of OBs [33]. We did not find such trend in aged $Optn^{-/-}$ OCs. The discrepancy is possibly due to different disease models between the studies. IL-6, which was increased in the measles virus model of

PDB, is associated with viral infection [34]. Our *Optn*$^{-/-}$ PDB model is virus-free and exhibits age-dependent pagetic lesions in a reminiscent to the clinical manifestations of PDB, highlighting the critical role of aging in the pathogenesis of PDB. By treating young or aged *Optn*$^{-/-}$ OBs with α-MEM-FBS containing secretions from age-matched *Optn*$^{-/-}$ OCs, we observed notable differences in OBs activity between young and aged *Optn*$^{-/-}$ cells, suggesting altered OBs activity modulated by OC secretions over age. Such findings provide a plausible mechanism for the age-dependent skeletal phenotypes observed. OC CM normalized the osteogenic capability of *Optn*$^{-/-}$ BMSCs in younger mice, explaining the absence of profound skeletal phenotypes. However, in older mice, OC CM significantly increased the osteogenic capability of *Optn*$^{-/-}$ BMSCs, suggesting overactive OBs in advanced PDB.

We further revealed the involvement of the TGF-β/BMP signaling pathway in BMSCs treated with OC conditioned media from aged *Optn*$^{-/-}$ mice. Our data indicate that deletion of *Optn* in OCs enhanced their osteogenic modulatory functions through cellular secretion. TGF-β signaling plays critical roles in skeletal development and homeostasis, and intersects with several key signaling pathways, such as BMP, Wnt, Hedgehog, Notch, and fibroblast growth factors (FGF) [35-39], to promote osteogenesis in OBs [35]. Secreted by OBs, TGF-β and BMPs are both members of the TGF-β superfamily of growth factors that affect both OB and OC functions, and therefore these factors play a critical role in the regulation of bone remodeling [25, 40]. In the current work, TGF-β/BMP signaling is implicated in this process based on gene expression studies, but additional experiments are necessary to identify factors secreted from OCs.

In conclusion, our study provides new insights into the abnormal bone remodeling observed in PDB. We demonstrate that hyperactive OCs regulate the osteogenic potential of BMSCs, potentially promoting increased osteoblastogenesis in advanced stages of PDB, which explains the trabecular and cortical bone phenotypes observed. The TGF-β/BMP signaling pathway may play a role in this process. Our findings contribute to a better understanding of the functions of OPTN and its impact on OBs in the context of PDB.

Supplementary Material

Refer to Web version on PubMed Central for supplementary material.

Acknowledgements

This work was supported by NIH/NIDCR [Grant Number R01DE022816, Ching-Chang Ko]. We thank Dr. Jie Liu from the Ohio State University College of Dentistry for micro-CT scanning. We thank Campus Microscopy and Imaging Facility (CMIF) at the Ohio State University for assistance with confocal microscopy. All authors gave final approval and agree to be accountable for all aspects of the work in ensuring that questions relating to the accuracy or integrity of any part of the work are appropriately investigated and resolved.

Data availability

Data will be made available on request.

References

[1]. Singer FR, Paget's disease of bone-genetic and environmental factors, Nat Rev Endocrinol 11(11) (2015) 662–71. [PubMed: 26284446]

[2]. Cundy T, Is the prevalence of Paget's disease of bone decreasing?, J Bone Miner Res 21 Suppl 2 (2006) P9–13. [PubMed: 17229016]

[3]. Ralston SH, Langston AL, Reid IR, Pathogenesis and management of Paget's disease of bone, Lancet 372(9633) (2008) 155–163. [PubMed: 18620951]

[4]. Albagha OM, Visconti MR, Alonso N, Langston AL, Cundy T, Dargie R, Dunlop MG, Fraser WD, Hooper MJ, Isaia G, Nicholson GC, del Pino Montes J, Gonzalez-Sarmiento R, di Stefano M, Tenesa A, Walsh JP, Ralston SH, Genome-wide association study identifies variants at CSF1, OPTN and TNFRSF11A as genetic risk factors for Paget's disease of bone, Nat Genet 42(6) (2010) 520–4. [PubMed: 20436471]

[5]. Singer FR, The etiology of Paget's disease of bone: viral and genetic interactions, Cell Metab 13(1) (2011) 5–6. [PubMed: 21195342]

[6]. Wong SW, Huang BW, Hu X, Ho Kim E, Kolb JP, Padilla RJ, Xue P, Wang L, Oguin TH 3rd, Miguez PA, Tseng HC, Ko CC, Martinez J, Global deletion of Optineurin results in altered type I IFN signaling and abnormal bone remodeling in a model of Paget's disease, Cell Death Differ 27(1) (2020) 71–84. [PubMed: 31076632]

[7]. Xue P, Hu X, Chang E, Wang L, Chen M, Wu TH, Lee DJ, Foster BL, Tseng HC, Ko CC, Deficiency of optineurin enhances osteoclast differentiation by attenuating the NRF2-mediated antioxidant response, Exp Mol Med 53(4) (2021) 667–680. [PubMed: 33864025]

[8]. Hu X, Wong SW, Liang K, Wu TH, Wang S, Wang L, Liu J, Yamauchi M, Foster BL, Ting JP, Zhao B, Tseng HC, Ko CC, Optineurin regulates NRF2-mediated antioxidant response in a mouse model of Paget's disease of bone, Sci Adv 9(4) (2023) eade6998. [PubMed: 36706179]

[9]. Ralston SH, Layfield R, Pathogenesis of Paget disease of bone, Calcif Tissue Int 91(2) (2012) 97–113. [PubMed: 22543925]

[10]. Daroszewska A, Ralston SH, Mechanisms of disease: genetics of Paget's disease of bone and related disorders, Nat Clin Pract Rheumatol 2(5) (2006) 270–7. [PubMed: 16932700]

[11]. Paul Tuck S, Layfield R, Walker J, Mekkayil B, Francis R, Adult Paget's disease of bone: a review, Rheumatology (Oxford) 56(12) (2017) 2050–2059. [PubMed: 28339664]

[12]. Appelman-Dijkstra NM, Papapoulos SE, Paget's disease of bone, Best Pract Res Clin Endocrinol Metab 32(5) (2018) 657–668. [PubMed: 30449547]

[13]. Rai NP, Anekar J, Mustafa SM, Devang Divakar D, Paget's disease with craniofacial and skeletal bone involvement, BMJ Case Rep 2016 (2016).

[14]. Liu ZZ, Hong CG, Hu WB, Chen ML, Duan R, Li HM, Yue T, Cao J, Wang ZX, Chen CY, Hu XK, Wu B, Liu HM, Tan YJ, Liu JH, Luo ZW, Zhang Y, Rao SS, Luo MJ, Yin H, Wang YY, Xia K, Xu L, Tang SY, Hu RG, Xie H, Autophagy receptor OPTN (optineurin) regulates mesenchymal stem cell fate and bone-fat balance during aging by clearing FABP3, Autophagy 17(10) (2021) 2766–2782. [PubMed: 33143524]

[15]. Munitic I, Giardino Torchia ML, Meena NP, Zhu G, Li CC, Ashwell JD, Optineurin insufficiency impairs IRF3 but not NF-kappaB activation in immune cells, J Immunol 191(12) (2013) 6231–40. [PubMed: 24244017]

[16]. Slowicka K, Vereecke L, Mc Guire C, Sze M, Maelfait J, Kolpe A, Saelens X, Beyaert R, van Loo G, Optineurin deficiency in mice is associated with increased sensitivity to Salmonella but does not affect proinflammatory NF-kappaB signaling, Eur J Immunol 46(4) (2016) 971–80. [PubMed: 26677802]

[17]. Mizuno N, Iwata T, Ohsawa R, Ouhara K, Matsuda S, Kajiya M, Matsuda Y, Kume K, Tada Y, Morino H, Yoshimoto T, Ueki Y, Mihara K, Sotomaru Y, Takeda K, Munenaga S, Fujita T, Kawaguchi H, Shiba H, Kawakami H, Kurihara H, Optineurin regulates osteoblastogenesis through STAT1, Biochem Biophys Res Commun 525(4) (2020) 889–894. [PubMed: 32171527]

[18]. Kim JM, Lin C, Stavre Z, Greenblatt MB, Shim JH, Osteoblast-Osteoclast Communication and Bone Homeostasis, Cells 9(9) (2020).

[19]. Obaid R, Wani SE, Azfer A, Hurd T, Jones R, Cohen P, Ralston SH, Albagha OME, Optineurin Negatively Regulates Osteoclast Differentiation by Modulating NF-kappaB and Interferon Signaling: Implications for Paget's Disease, Cell Rep 13(6) (2015) 1096–1102. [PubMed: 26527009]

[20]. Qian H, Badaloni A, Chiara F, Stjernberg J, Polisetti N, Nihlberg K, Consalez GG, Sigvardsson M, Molecular characterization of prospectively isolated multipotent mesenchymal progenitors provides new insight into the cellular identity of mesenchymal stem cells in mouse bone marrow, Mol Cell Biol 33(4) (2013) 661–77. [PubMed: 23184664]

[21]. Wang L, Liang Y, Zhou X, Tian Y, Miao Z, Ko CC, Hu X, Nrf2 differentially regulates osteoclast and osteoblast differentiation for bone homeostasis, Biochem Biophys Res Commun 674 (2023) 19–26. [PubMed: 37393640]

[22]. Wang L, Wu TH, Hu X, Liu J, Wu D, Miguez PA, Wright JT, Zhang S, Chi JT, Tseng HC, Ko CC, Biomimetic polydopamine-laced hydroxyapatite collagen material orients osteoclast behavior to an anti-resorptive pattern without compromising osteoclasts' coupling to osteoblasts, Biomater Sci 9(22) (2021) 7565–7574. [PubMed: 34664567]

[23]. Sims NA, Martin TJ, Osteoclasts Provide Coupling Signals to Osteoblast Lineage Cells Through Multiple Mechanisms, Annu Rev Physiol 82 (2020) 507–529. [PubMed: 31553686]

[24]. Miyazono K, Kamiya Y, Morikawa M, Bone morphogenetic protein receptors and signal transduction, J Biochem 147(1) (2010) 35–51. [PubMed: 19762341]

[25]. Wu M, Chen G, Li YP, TGF-beta and BMP signaling in osteoblast, skeletal development, and bone formation, homeostasis and disease, Bone Res 4 (2016) 16009. [PubMed: 27563484]

[26]. Kravets I, Paget's Disease of Bone: Diagnosis and Treatment, Am J Med 131(11) (2018) 1298–1303. [PubMed: 29752905]

[27]. Lalam RK, Cassar-Pullicino VN, Winn N, Paget Disease of Bone, Semin Musculoskelet Radiol 20(3) (2016) 287–299. [PubMed: 27741544]

[28]. Silva IAL, Conceicao N, Gagnon E, Brown JP, Cancela ML, Michou L, Molecular effect of an OPTN common variant associated to Paget's disease of bone, PLoS One 13(5) (2018) e0197543. [PubMed: 29782529]

[29]. Silva IAL, Conceicao N, Gagnon E, Caiado H, Brown JP, Gianfrancesco F, Michou L, Cancela ML, Effect of genetic variants of OPTN in the pathophysiology of Paget's disease of bone, Biochim Biophys Acta Mol Basis Dis 1864(1) (2018) 143–151. [PubMed: 28993189]

[30]. Ralston SH, Clinical practice. Paget's disease of bone, N Engl J Med 368(7) (2013) 644–50. [PubMed: 23406029]

[31]. Rachner TD, Khosla S, Hofbauer LC, Osteoporosis: now and the future, Lancet 377(9773) (2011) 1276–87. [PubMed: 21450337]

[32]. Obaid R, Wani SE, Azfer A, Hurd T, Jones R, Cohen P, Ralston SH, Albagha OME, Optineurin Negatively Regulates Osteoclast Differentiation by Modulating NF-κB and Interferon Signaling: Implications for Paget's Disease, Cell Reports 13(6) (2015) 1096–1102. [PubMed: 26527009]

[33]. Teramachi J, Nagata Y, Mohammad K, Inagaki Y, Ohata Y, Guise T, Michou L, Brown JP, Windle JJ, Kurihara N, Roodman GD, Measles virus nucleocapsid protein increases osteoblast differentiation in Paget's disease, J Clin Invest 126(3) (2016) 1012–22. [PubMed: 26878170]

[34]. Velazquez-Salinas L, Verdugo-Rodriguez A, Rodriguez LL, Borca MV, The Role of Interleukin 6 During Viral Infections, Front Microbiol 10 (2019) 1057. [PubMed: 31134045]

[35]. Chen G, Deng C, Li YP, TGF-beta and BMP signaling in osteoblast differentiation and bone formation, Int J Biol Sci 8(2) (2012) 272–88. [PubMed: 22298955]

[36]. Johnson RW, Nguyen MP, Padalecki SS, Grubbs BG, Merkel AR, Oyajobi BO, Matrisian LM, Mundy GR, Sterling JA, TGF-beta promotion of Gli2-induced expression of parathyroid hormone-related protein, an important osteolytic factor in bone metastasis, is independent of canonical Hedgehog signaling, Cancer Res 71(3) (2011) 822–31. [PubMed: 21189326]

[37]. Kluppel M, Wrana JL, Turning it up a Notch: cross-talk between TGF beta and Notch signaling, Bioessays 27(2) (2005) 115–8. [PubMed: 15666349]

[38]. Meng X, Vander Ark A, Lee P, Hostetter G, Bhowmick NA, Matrisian LM, Williams BO, Miranti CK, Li X, Myeloid-specific TGF-beta signaling in bone promotes basic-FGF and breast cancer bone metastasis, Oncogene 35(18) (2016) 2370–8. [PubMed: 26279296]

[39]. Weivoda MM, Ruan M, Pederson L, Hachfeld C, Davey RA, Zajac JD, Westendorf JJ, Khosla S, Oursler MJ, Osteoclast TGF-beta Receptor Signaling Induces Wnt1 Secretion and Couples Bone Resorption to Bone Formation, J Bone Miner Res 31(1) (2016) 76–85. [PubMed: 26108893]

[40]. Al Nofal AA, Altayar O, BenKhadra K, Qasim Agha OQ, Asi N, Nabhan M, Prokop LJ, Tebben P, Murad MH, Bone turnover markers in Paget's disease of the bone: A Systematic review and meta-analysis, Osteoporos Int 26(7) (2015) 1875–91. [PubMed: 26037791]

Highlights

- Pagetic alterations exhibit in the trabecular bones of aged *Optn*$^{-/-}$ mice.
- Altered osteoblast (OB) activity may contribute to such pagetic phenotypes.
- Osteoclast (OC) secretions increase OB activity in aged *Optn*$^{-/-}$ mice *in vitro*.
- *Optn*$^{-/-}$ OC secretions activate TGF-β/BMP signaling in aged *Optn*$^{-/-}$ OB cells.

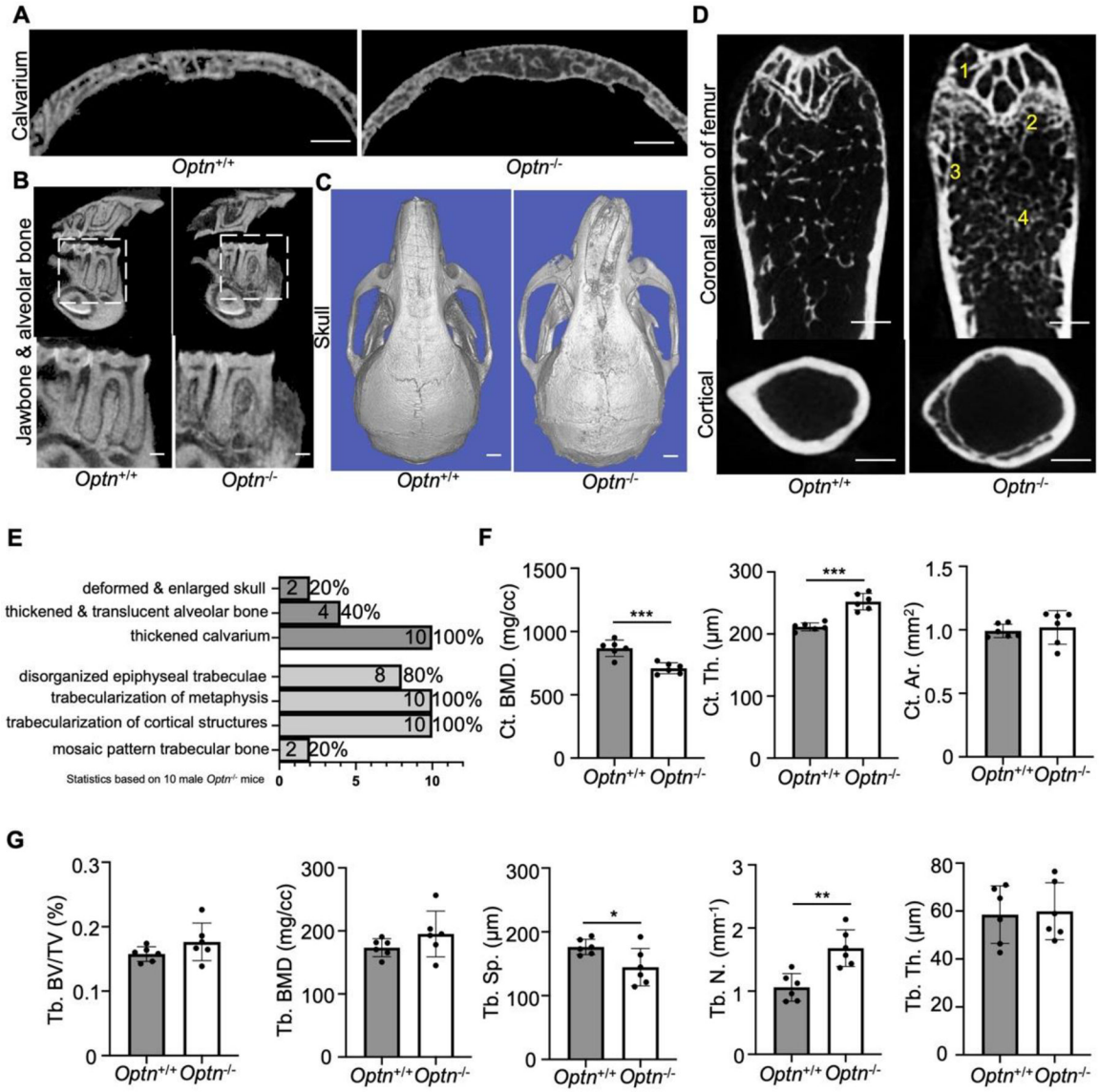

Figure 1.

Deletion of *Optn* contributes to trabecular pagetic alterations in skulls and femurs of aged mice. (A-B) Representative 2D micro-CT renderings showed (A) thickened calvarium (coronal section), (B) translucent and mosaic trabecular of jawbone and mandibular alveolar bone (sagittal section) in 24-month-old $Optn^{+/+}$ compared to $Optn^{-/-}$ mice. Scale bars, 500 μm. (C) Representative 3D reconstruction images showed deformed and enlarged skull in 24-month-old $Optn^{+/+}$ compared to $Optn^{-/-}$ mice. Scale bars, 1 mm. (D) Representative 2D micro-CT renderings of femurs (coronal section) and cortical bone regions (cross section at middle shaft) of 24-month-old $Optn^{+/+}$ and $Optn^{-/-}$ mice showed 1) disorganized epiphyseal trabeculae, 2) trabecularization of metaphysis, 3) trabecularization of cortical structures, and 4) mosaic pattern trabecular bone in $Optn^{-/-}$ mice. Scale bars, 500 μm. (E) Phenotypic analysis of craniofacial (top) and femur trabecular abnormalities in 24-month-old $Optn^{-/-}$ mice. Statistics are based on 10 male $Optn^{-/-}$ mice. (F) Micro-CT measurements of trabecular bone value fraction (Tb. BV/TV), trabecular bone mineral density (Tb. BMD),

trabecular spacing (Tb. Sp), trabecular number (Tb. N), and trabecular thickness (Tb. Th). n = 6 per genotype. Data presented as mean ± SD. *$P < 0.05$, **$P<0.01$. (G) Micro-CT measurements of cortical bone mineral density (Ct. BMD), cortical thickness (Ct. Th), and cortical area (Ct. Ar). n = 6 per genotype. Data presented as mean ± SD. ***$P < 0.001$.

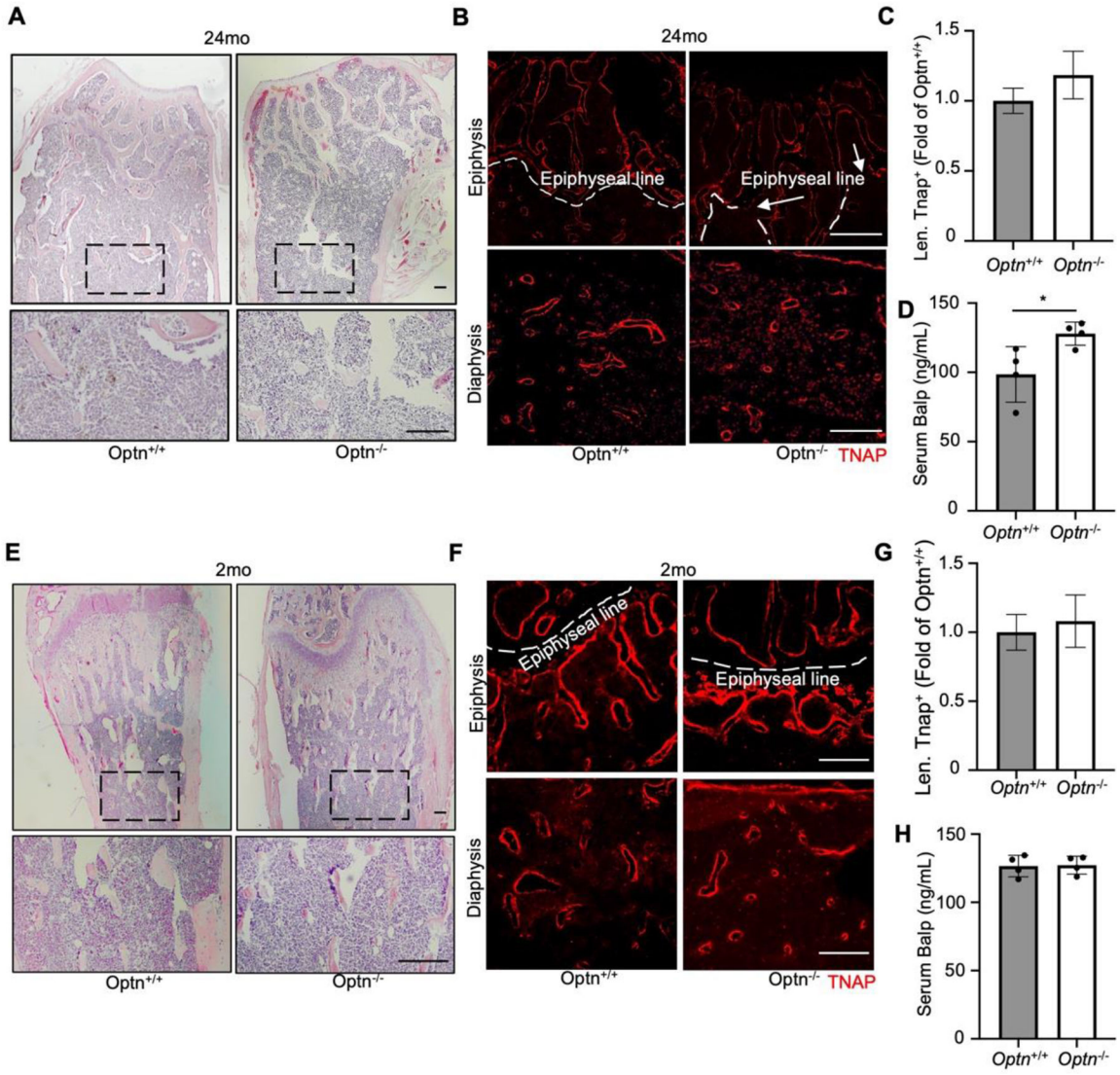

Figure 2.

Deletion of *Optn* leads to altered OBs activity in aged but not young mice. (A) Representative H&E images from metaphyses and diaphyses of femurs from 24-month-old showing irregular epiphysis and smaller in trabeculae in aged $Optn^{-/-}$ mouse. Scale bars, 100 μm. (B) Representative imaging of TNAP staining for 24-month-old $Optn^{+/+}$ and $Optn^{-/-}$ mouse femurs. Scale bars, 200 μm. Arrows indicates discontinued epiphyseal line. Increased TNAP localization was observed in the spaces between trabeculae in aged $Optn^{-/-}$ mice (C) Quantification of length of TNAP positive (Alp^{+}) signal, n = 4 per genotype. Data presented as mean ± SD. $^{*}P < 0.05$. (D) ELISA assay on serum BALP level of 24-month-old $Optn^{+/+}$ and $Optn^{-/-}$ mice. n=4 mice. Data presented as mean ± SD. $^{*}P < 0.05$. (E) Representative H&E images from metaphyses and diaphyses of femurs of 2-month-old $Optn^{+/+}$ and $Optn^{-/-}$ mouse. Scale bars, 100 μm. (F) Representative imaging of TNAP staining for 2-month-old $Optn^{+/+}$ and $Optn^{-/-}$ mouse femurs. Scale bars, 200 μm. (G) Quantification of length of TNAP positive (Alp^{+}) signal. n = 4 per genotype. (H) ELISA assay for serum BALP levels of 2-month-old $Optn^{+/+}$ and $Optn^{-/-}$ mice. n=4 mice.

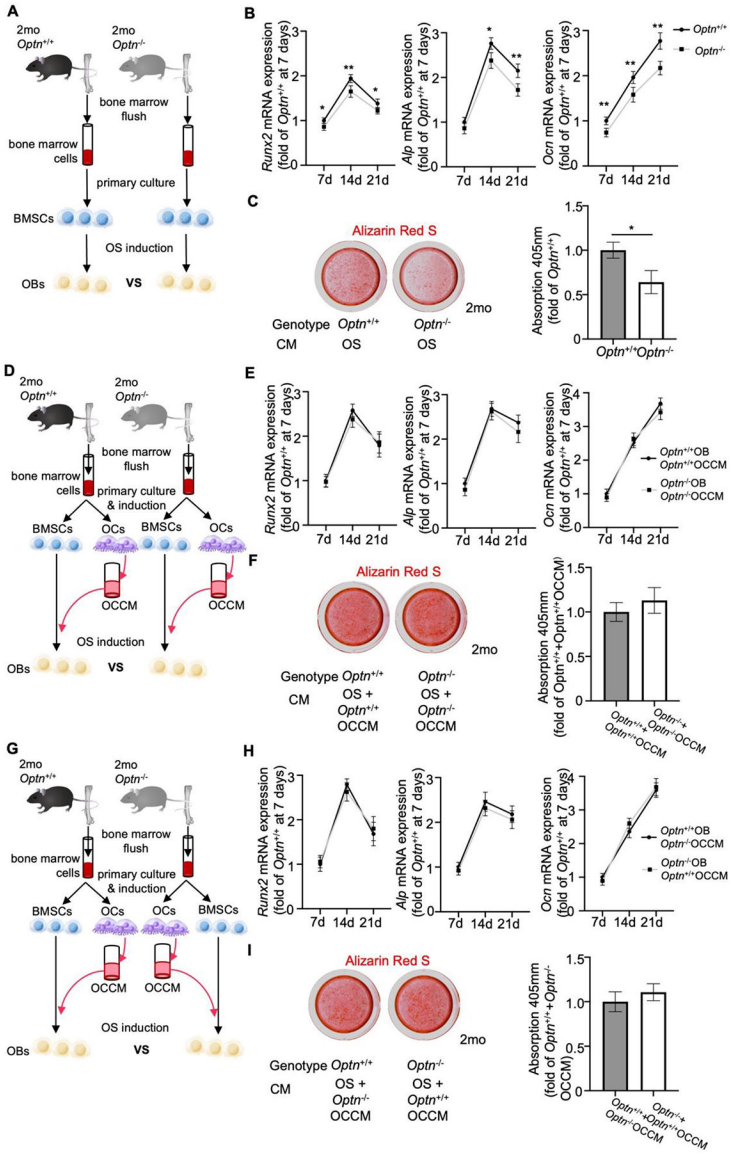

Figure 3.

Osteoclast secreted factors restore compromised *in vitro* osteogenic induction of BMSCs from young $Optn^{-/-}$ mice. (A) Schematic for the cell culture experiment to compare osteogenic potential of BMSCs from 2-month-old $Optn^{+/+}$ and $Optn^{-/-}$ mice. (B) qPCR analysis of OB markers, *Runx2*, *Alpl*, and *Bglap/Ocn* in BMSCs from 2-month-old $Optn^{+/+}$ and $Optn^{-/-}$ mice during osteogenic induction at 7, 14, and 21d. Data were normalized to actin (*Actb*). n = 3 replicates. Data presented as mean ± SD. $*P < 0.05$, $**P < 0.01$. (C) Representative images and quantification of Alizarin Red S staining in $Optn^{+/+}$ and $Optn^{-/-}$ BMSCs at 21d of osteogenic induction. Data presented as mean ± SD. $*P < 0.05$, $**P < 0.01$. (D) Schematic for the cell culture experiment to compare the osteogenic potential of BMSCs from 2-month-old $Optn^{+/+}$ and $Optn^{-/-}$ mice treated with OC CM from the cells of the same genotype. (E) qPCR analysis of OB markers, *Runx2*, *Alpl*, and *Bglap/Ocn* in BMSCs from 2-month-old $Optn^{+/+}$ and $Optn^{-/-}$ mice during osteogenic induction at 7,

14, and 21d, and treated with OC CM from the cells of the same genotype. Data were normalized to actin (*Actb*). n = 3 replicates. (F) Representative images and quantification of Alizarin Red S staining in *Optn*$^{+/+}$ and *Optn*$^{-/-}$ BMSCs at 21d of osteogenic induction and treated with OC CM from the cells of the same genotype. (G) Schematic for the cell culture experiment to compare the osteogenic potential of BMSCs from 2-month-old *Optn*$^{+/+}$ and *Optn*$^{-/-}$ mice treated with OC CM from the cells of the other genotype. (H) qPCR analysis of OB markers, *Runx2*, *Alpl*, and *Bglap/Ocn* in BMSCs from 2-month-old *Optn*$^{+/+}$ and *Optn*$^{-/-}$ mice during osteogenic induction at 7, 14, and 21d, and treated with OC CM from the cells of the same genotype. Data were normalized to actin (*Actb*). n = 3 replicates. (I) Representative images and quantification of Alizarin Red S staining in *Optn*$^{+/+}$ and *Optn*$^{-/-}$ BMSCs at 21d of osteogenic induction and treated with OC CM from the cells of the other genotype.

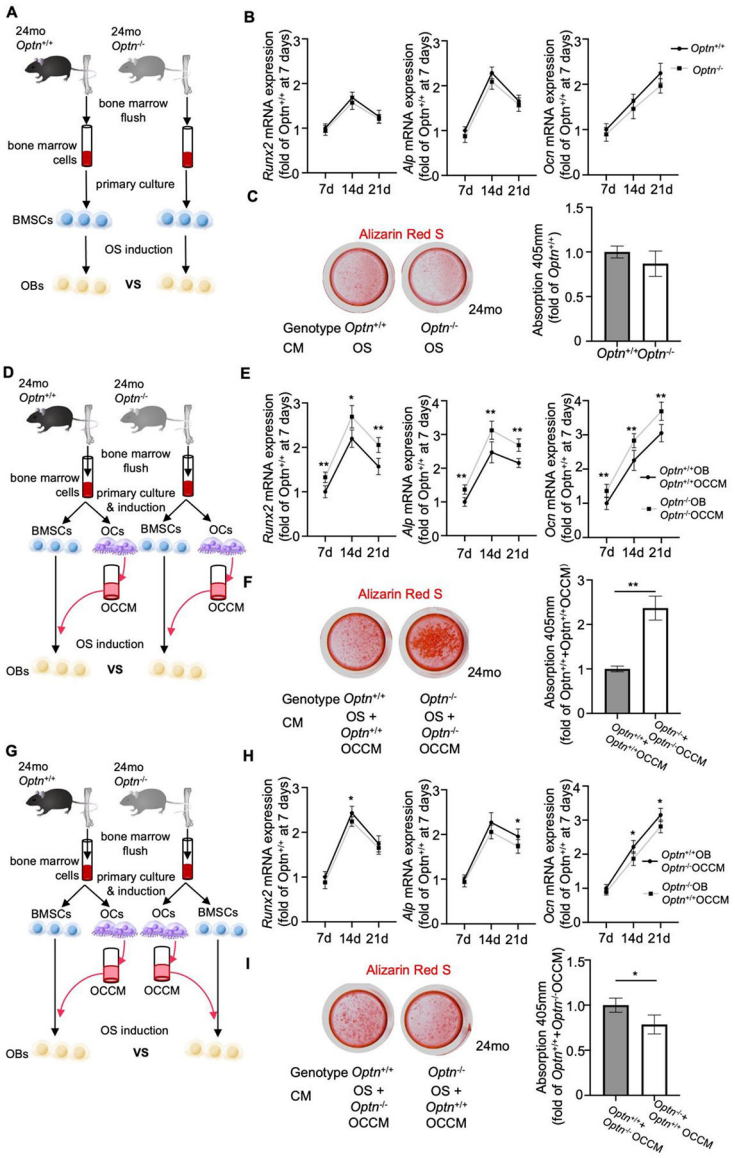

Figure 4.

Osteoclastic secretion increases osteogenic activity of BMSCs in aged *Optn*$^{-/-}$ mice. (A) Schematics for the cell culture rational to compare the osteogenic potential of BMSCs from 24-month-old *Optn*$^{+/+}$ and *Optn*$^{-/-}$ mice. (B) qPCR analysis of osteogenic genes, *Runx2*, *Alp*, and *Ocn* in BMSCs from 24-month-old *Optn*$^{+/+}$ and *Optn*$^{-/-}$ mice during osteogenesis at 7d, 14d, and 21d respectively, data were normalized to actin. n = 3 replicates. (C) Representative imaging and quantification of Alizarin Red S staining on osteogenic-induced BMSCs at 21d. (D) Schematics for the cell culture rational to compare the osteogenic potential of BMSCs from 24-month-old *Optn*$^{+/+}$ and *Optn*$^{-/-}$ mice treated with (pre)OC conditioned media (CM) from the cells of the same genotype. (E) qPCR analysis of osteogenic genes, *Runx2*, *Alp*, and *Ocn* in BMSCs from 2-month-old *Optn*$^{+/+}$ and *Optn*$^{-/-}$ mice treated with OC CM obtained from osteoclasts of the same mice during osteogenesis at 7d, 14d, and 21d respectively, data were normalized to actin. n = 3 replicates. Data presented

as mean ± SD. *p < 0.05, **p < 0.01. (F) Representative imaging and quantification of Alizarin Red S staining on osteogenic-induced BMSCs at 21d. Data presented as mean ± SD. **p < 0.01. (G) Schematics for the cell culture rational to compare the osteogenic potential of BMSCs from 24-month-old *Optn*$^{+/+}$ and *Optn*$^{-/-}$ mice treated with (pre)OC CM from the cells of the other genotype. (H) qPCR analysis of osteogenic genes, *Runx2*, *Alp*, and *Ocn* in BMSCs from 2-month-old *Optn*$^{+/+}$ and *Optn*$^{-/-}$ mice treated with osteoclast conditioned media obtained from osteoclasts of the mice of the opposite genotype during osteogenesis at 7d, 14d, and 21d respectively, data were normalized to actin. n = 3 replicates. Data presented as mean ± SD. *p < 0.05. (I) Representative imaging and quantification of Alizarin Red S staining on osteogenic-induced BMSCs at 21d. Data presented as mean ± SD. *p < 0.05.

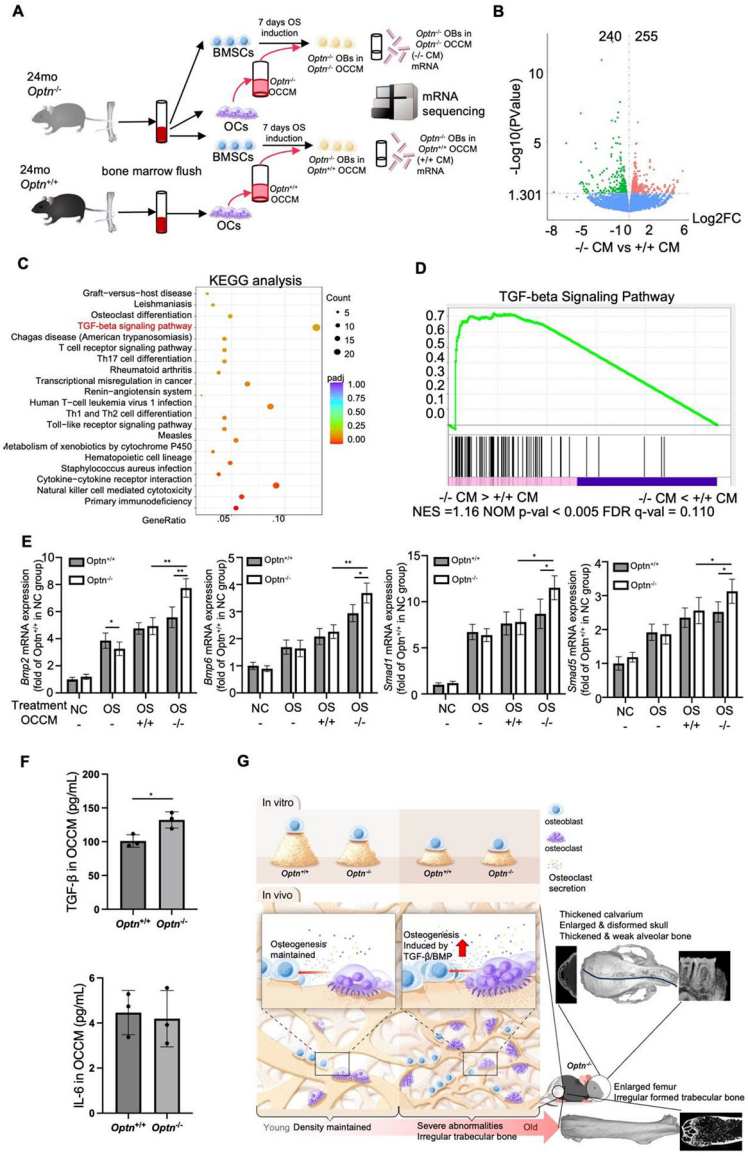

Figure 5.

Osteoclast secreted factors trigger TGF-β pathway signaling in aged *Optn*$^{-/-}$ mice. (A) Schematic for the RNA-seq experiments to analyze the gene expressions in the osteogenic-induced BMSCs from 24-month-old *Optn*$^{-/-}$ mice treated with conditioned media from osteoclasts of either 24-month-old *Optn*$^{+/+}$ or *Optn*$^{-/-}$ mice. (B) Volcano plots showed differential expression (DE) of genes in BMSCs from 24-month-old *Optn*$^{-/-}$ mice treated with OC CM from *Optn*$^{-/-}$ vs. *Optn*$^{+/+}$ mice. 255 genes were upregulated and 240 genes were downregulated. n = 3 per genotype. (C) Kyoto Encyclopedia of Genes and Genomes (KEGG) analysis for RNA-seq analysis of osteogenic-induced BMSCs from 24-month-old *Optn*$^{-/-}$ mice treated with OC CM from *Optn*$^{+/+}$ or *Optn*$^{-/-}$ mice. (D) Gene set enrichment analysis (GSEA) reveals TGF-β signaling pathway related genes are mostly enriched. NES = 1.16, $P < 0.005$, q = 0.110. (E) qPCR analysis of genes in TGF-β signaling pathway, *Mbp2*, *Mbp6*, *Smad1*, and *Smad5* in BMSCs from 24-month-old *Optn*$^{+/+}$ and *Optn*$^{-/-}$ mice

treated in different settings, data were normalized to actin (*Actb*). n = 3 replicates. Data presented as mean ± SD. **P* < 0.05, ***P* < 0.01. (F) ELISA assay for TGF- β and IL-6 levels in OC CM collected from 24-month-old $Optn^{+/+}$ and $Optn^{-/-}$ osteoclasts. n=3. (G) Schematic illustration summarizing that deletion of OPTN results in decreased osteogenic activity in OB *in vitro* regardless of age. In young $Optn^{-/-}$ bones, OC secretion maintains normal OB osteogenic activity and bone density. In aged $Optn^{-/-}$ bones, increased OC secretion triggers TGF-β/BMP signaling in OB, which results in abnormally regulated osteogenesis and trabecular abnormalities in skull and femur.